THE JOURNAL OF PHYSICAL CHEMISTRY B

Article

pubs.acs.org/JPCB

Discrimination of 4-Hydroxyproline Diastereomers by Vibrational Spectroscopy of the Gaseous Protonated Species

Maria Elisa Crestoni,*[,†] Barbara Chiavarino,[†] Debora Scuderi,[‡] Annito Di Marzio,[†] and Simonetta Fornarini[†]

[†]Dipartimento di Chimica e Tecnologie del Farmaco, Università di Roma "La Sapienza", P. le A. Moro 5, I-00185 Roma, Italy

[‡]Laboratoire de Chimie Physique d'Orsay, Université Paris-Sud 11, Batiment 350-Campus d'Orsay 15, avenue Jean Perrin, 91405 Orsay Cedex, France

Supporting Information

ABSTRACT: Hydroxylation of proline is a prominent oxidative post-translational modification (oxPTM) in animals, characterized by site specificity and stereochemical control. The presence of this irreversible modification and the ensuing generation of a chiral center have been assayed in (2*S*,4*R*)-4-hydroxyproline and (2*S*,4*S*)-4-hydroxyproline forming the protonated species by electrospray ionization and sampling them by infrared multiple photon dissociation (IRMPD) spectroscopy. IRMPD spectra, recorded both in the 950−1950 cm^{-1} (using the CLIO free electron laser) and in the 3200−3700 cm^{-1} [using a tabletop parametric oscillator/amplifier (OPO/OPA) laser] regions, have been interpreted by comparison with the absorbance spectra of the lowest energy structures calculated at MP2/6-311+G** level of theory. Remarkable spectral differences have emerged in the fingerprint region, pointing to the unambiguous discrimination between *S*,*R* and *S*,*S* diastereomers. The main differences arise from the position of the carbonyl stretching mode, a signature of nonzwitterionic structures, moving from 1750 cm^{-1} for the *S*,*R* form to 1770 cm^{-1} for the *S*,*S* diastereomer. Furthermore, a well-defined band associated with the NH_2 wagging mode at 1333 cm^{-1} is a distinct mark of the *S*,*S* isomer. Each gaseous protonated epimer comprises a population of at least three conformers, stabilized by intramolecular hydrogen bonds linking the two hydrogens of protonated secondary amine group with the 4-hydroxy substituent and with an oxygen atom of the carboxylic group, respectively. Interestingly, a tendency to adopt either C(4)-*exo* (up) or C(4)-*endo* (down) pyrrolidine puckering upon proline 4(*R*)- or 4(*S*)-hydroxylation, respectively, is observed here. The same bias is found in neutral hydroxyprolines and in collagen model peptides. In the protonated species under examination, this bias originates chirality-induced vibrational features revealed by IRMPD spectroscopy.

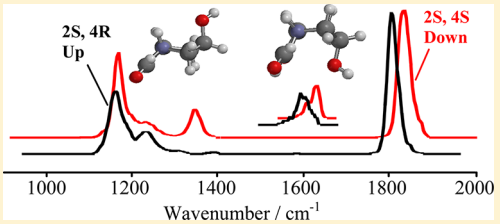

1. INTRODUCTION

The molecular basis of collagen structure and stability has become the subject of extensive studies aimed at elucidating its (dis)functions and at developing new biocompatible functional materials.[1−7] Collagen is the most abundant protein in mammals and consists of parallel strands folded in tight triple helices, each chain containing a X−Y−Gly repeat with amide bonds in a trans conformation. A proline (Pro) amino acid is usually found in the X-position, and its (2*S*,4*R*)-4-hydroxyproline (Hyp) variant is in the Y-position.[8] Enzymatic 4*R*-hydroxylation of proline,[9] where the hydroxyl group is installed only in proline residues in the Y-position of protocollagen chains, is a prevalent oxidative post-translational modification (oxPTM),[10] which significantly enhances the thermal stability of the triple helix.[11] Conversely, the formation of (2*S*,4*S*)-4-hydroxyproline (hyp) diastereomer is severely destabilizing and has not been observed in natural proteins.[12]

The subtle perturbation introduced by hydroxylation of the proline residue has not been easy to identify in intact proteins until recently when a high-resolution mass spectrometric assay unveiled its broad occurrence and involvement in protein folding and redox signaling mechanisms.[13,14] X-ray structures have revealed that the flexible pyrrolidine ring of proline and hydroxyproline adopts an alternation of C(4)-*endo* and C(4)-*exo* bent conformations in the X- and Y-positions, respectively, of the collagen chains.[15,16]

Proline derivatives introduced in model peptides have evidenced the critical role of the intrastrand hydrogen bonds,[17] of dipole−dipole interactions,[18] and, as a result of stereoelectronic effects, of the pyrrolidine ring puckering for the conformational stability of the collagen triple helix.[16,19] In particular, the stereoelectronic effect, so-called "gauche" effect,[20,21] exerted by the electronegative 4*R*-OH substituent, imposes a C(4)-*exo* pyrrolidine ring pucker in Hyp and preorganizes the backbone torsion angles in the Y-position, so enhancing triple helix stability at physiological temperatures. The inverse effect is verified with the 4*S* diastereomer, hyp, which adopts a C(4)-*endo* pucker and stabilizes model peptides when incorporated in the X-position, in agreement with the opposite stereoelectronic preference of X- and Y-positions. This

Received: March 12, 2012
Revised: July 3, 2012
Published: July 5, 2012

   dx.doi.org/10.1021/jp302382p | *J. Phys. Chem. B* 2012, 116, 8771−8779

situation is, however, not found in natural collagen, because of unfavorable interactions of the 4-hydroxy group with the adjacent strand.[22]

Replacing hydroxyl groups with fluorine atoms, which elicits the largest inductive effect, has enabled the synthesis of collagen mimetics triple helices endowed with hyperstability when (2*S*,4*R*)-4-fluoroproline (Flp) and (2*S*,4*S*)-4-fluoroproline (flp) occupy the Y- and X-positions, respectively.[23] Interestingly, merely steric effects largely prevail when the 4-substituent is a methyl group so that the pair of 4-methylproline epimers displays a reversed balance for the conformational equilibrium illustrated in Scheme 1 when compared with the F and OH substituents.[24]

Scheme 1. Conformational Equilibria of 4-Substituted Prolines (Preferred Conformer Indicated for Each Substitution Pattern)

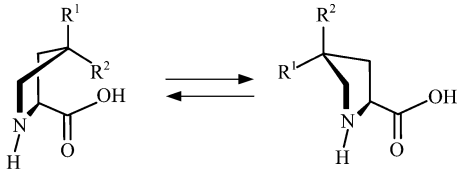

C^{γ}-endo pucker C^{γ}-exo pucker

R^1 = H, R^2 = OH (hyp) R^1 = OH, R^2 = H (Hyp)
R^1 = H, R^2 = F (flp) R^1 = F, R^2 = H (Flp)
R^1 =CH_3, R^2 = H (mep) R^1 = H, R^2 = CH_3 (Mep)

The conformational flexibility of Pro and of its derivates has been investigated by experimental[25−30] and theoretical tools.[31−38] Among the several conformers identified in the gas phase within a narrow energy range, however, just the two most stable forms have been identified for neutral Pro and for both 4(*S*)- and 4(*R*)-hydroxyproline by rotational spectroscopy in supersonic jet, under conditions where efficient collisional cooling of high-energy conformers is operative.[39] While neutral proline occurs in both the lowest energy *endo* (global minimum) and the *exo* forms stabilized by an intramolecular N···H−O hydrogen bond,[40] each neutral 4(*R*)- and 4(*S*)-hydroxyproline adopts two either C(4)-*exo* or C(4)-*endo* puckering conformations, respectively, one of which may additionally benefit an intramolecular N−H···O═C hydrogen bond.

Recently, the molecular properties of isolated proline ions, namely, protonated proline,[41] the proton-bound dimer,[42] and proline tagged by various metal[43−45] or ammonium[46] ions, have been investigated in the gas phase, by means of IR multiple photon dissociation (IRMPD) spectroscopy. This methodology relies on the coupling of widely tunable sources of IR light with tandem mass spectrometry.[47] This relatively novel and highly efficient tool has allowed unveiling of the structural features of a variety of mass-selected ions[48−52] based on the photofragmentation induced by IR laser sources, such as the broadly used tabletop OPO/OPA device[53−55] or the IR free electron laser (FEL) at CLIO[56] or FELIX.[57] Both calculations and IRMPD spectroscopic experiments indicate that bare protonated proline adopts the charge solvation form, whereas in the proton-bound homodimer or in the complexes with metal ions, including sodium and barium, the salt bridge (zwitterionic) form has been demonstrated.

Herein, we present the first structural assay of protonated (2*S*,4*R*)- and (2*S*,4*S*)-hydroxyproline epimers ($HypH^+$ and $hypH^+$, respectively) in an isolated environment, so describing their inherent molecular features in the absence of complicating interactions with bulk solvent and counterions. The comparative investigation of $HypH^+$ and $hypH^+$ ions by electrospray ionization mass spectrometry (ESI-MS) coupled to IRMPD spectroscopy and density functional theory (DFT) calculations has been undertaken, aimed at unveiling the geometric determinants induced in native proline by the stereoselective 4-hydroxylation.

2. METHODS

All reagents were commercial products (Sigma-Aldrich srl Milan, Italy) and were used without purification. Protonated 4(*R*)-hydroxy-L-proline, $HypH^+$, and (4*S*)-hydroxy-L-proline ions, $hypH^+$, *m*/*z* 132, were generated by ESI by infusing a 4 μM solution of the amino acids dissolved in water/methanol (1:1) at a flow rate of 2 μL min^{-1}.

Energy-variable collision-induced dissociation (CID) experiments were carried out using a commercial hybrid triple quadrupole linear ion trap mass spectrometer (2000 Q TRAP Applied Biosystems), with a $Q1q2Q_{LIT}$ configuration (Q1, first mass analyzing quadrupole; q2, nitrogen-filled collision cell; and Q_{LIT}, linear ion trap). The electrosprayed sampled ions were mass selected by Q1 and collided with N_2 at 2.4−4.0 × 10^{-5} mbar in q2 at variable collision energies (E_{lab} = 5−50 V) for CID experiments. The ionic products were monitored by scanning Q_{LIT}. The systematic variation of the collision energy, converted to the center of mass frame ($E_{CM} = [m/(m + M)]$ E_{lab}, where *m* and *M* are the masses of the collision gas and of the ion, respectively) allows one to obtain breakdown curves yielding phenomenological appearance energies (E_{app}) for the various fragmentation channels.[58,59]

IR spectroscopy of mass-selected ions was performed employing two light sources. For the mid-IR range (950−1950 cm^{-1}), the CLIO FEL beamline coupled to a modified Paul-ion trap mass spectrometer (Bruker Esquire 3000+) was used.[60,61] A conical hole drilled in the ring electrode allowed optical access to the center of the trap. The FEL radiation is based on a 10−48 MeV electron linear accelerator and is delivered in 8 μs macropulses (25 Hz), each containing 500 micropulses (few picoseconds long). Typical macropulse energies are 40 mJ. For the present study, the electron energy was set to 44 MeV, and a stable average power of 800−900 mW was observed. The IR-FEL spectral width (fwhm) was less than 0.5% of the central wavelength.

The 3200−3700 cm^{-1} spectral region was investigated using an Optical Parametric Oscillator/Amplifier (OPO/OPA from LaserVision, Bellevue, WA) laser system, coupled to a modified Paul type quadrupole ion trap mass spectrometer (Bruker Esquire 6000+).[62] The parametric converter is pumped by an Nd:YAG laser (Continuum Surelite II) operating at 10 Hz repetition rate and delivering 600 mJ/pulse (4−6 ns long). In the investigated spectral range, the typical output pulse energy from the OPO/OPA laser source was 24 mJ/pulse, with a spectral bandwidth of about 3−4 cm^{-1}.

In the ion trap, the ions of interest were mass selected and accumulated for 20 ms prior to irradiation for 1 s. The laser wavelength was continuously moved at a speed of 0.1 cm^{-1} s^{-1}, and the mass spectrum was typically derived from an accumulation over four scans.

dx.doi.org/10.1021/jp302382p | J. Phys. Chem. B 2012, 116, 8771−8779

The only fragmentation channel observed upon irradiation of both $HypH^+$ and $hypH^+$ ions at active wavelengths yields an ion at m/z 86. The IRMPD spectrum is obtained by monitoring the photofragmentation efficiency R, defined as $-\ln[I_P/(I_P + I_F)]$, where I_P and I_F are the intensity of the precursor ion and of the fragment ion, respectively, as a function of the laser frequency.[57]

Quantum chemical calculations at the MP2/6-311+G** level of theory were carried out to obtain the geometries, energetics, and IR absorption spectra of the low-lying structures of $HypH^+$ and $hypH^+$. All calculations were performed using the Spartan 10 software package. The optimized structures were subjected to harmonic vibrational frequency analysis to characterize the stationary points as local minima.

Harmonic vibrational frequencies were scaled by 0.971 (0.945) in the 950−1950 cm^{-1} (3200−3700 cm^{-1}) spectral region, on the basis of the good agreement between the experimental and the computed frequencies.[63,64] All reported energies were corrected for scaled zero point energies. Theoretical IR stick spectra were convoluted with a Gaussian profile with an associated width (fwhm) of 20 cm^{-1} (5 cm^{-1}) in the 950−1950 cm^{-1} (3200−3700 cm^{-1}) frequency range for consistency with the experimental spectral resolution.

3. RESULTS AND DISCUSSION

3.1. Photodissociation and CID Mass Spectra. The selected $HypH^+$ and $hypH^+$ ions have been assayed by CID at variable energy in a hybrid triple quadrupole-linear ion trap mass spectrometer. Figure 1S in the Supporting Information shows the dependence of the relative abundances of the parent and fragment ions on the collision energy reported in the center-of-mass frame (E_{CM}). Both $HypH^+$ or $hypH^+$ ions were mass selected in the first quadrupole and submitted to energy-variable collisions with N_2 in the quadrupole collision sector. Loss of H_2O and CO leads to the formation of an ion at m/z 86 as the exclusive fragmentation route. The linear extrapolation of the rising portion of the breakdown curves yields a phenomenological appearance energy (E_{app}) of 1.10 ± 0.20 eV (106 ± 20 kJ mol^{-1}) and of 1.20 ± 0.20 eV (116 ± 20 kJ mol^{-1}) for the dissociation of $HypH^+$ and $hypH^+$, respectively, which are therefore both strongly bound isomers, barely differentiated upon CID measurements.

The ion at m/z 86 is also the only fragment from the two sampled species upon resonant IR excitation, which provides a slow heating of the sampled ions activating dissociation along the lowest energy pathway.[65,48] The threshold energy associated with this fragmentation channel, likely leading to an ion protonated at the secondary amine group, as commonly observed in CID and laser-induced dissociation of protonated amino acids,[66] requires the absorption of multiple (more than 3) photons to obtain a sizable photofragmentation yield even in the short wavelength region (3200−3600 cm^{-1}), where the energy of one photon is 38−43 kJ mol^{-1}.

Exemplary mass spectra recorded upon selection of either $HypH^+$ or $hypH^+$ before (a) and after (b) irradiation with OPO/OPA IR radiation on resonance at 3550 cm^{-1}, and with CLIO FEL light on resonance at 1770 cm^{-1}, are shown in Figures 2S and 3S in the Supporting Information, respectively.

3.2. IRMPD Spectra. IRMPD spectroscopy has recently shown the potential to distinguish between isomers and conformers of several (bio)molecular ions.[67−72] This aptitude is taken advantage of in the present study. When electrosprayed $HypH^+$ and $hypH^+$ ions, isolated in the Paul ion trap and irradiated with IR light, absorb resonant IR photons, their internal energy increases up to a dissociation threshold, and a wavelength-dependent photofragmentation process is observed. Experimental IRMPD spectra of $HypH^+$ and $hypH^+$ in the 950−1950 cm^{-1} wavenumber range are presented in Figure 1.

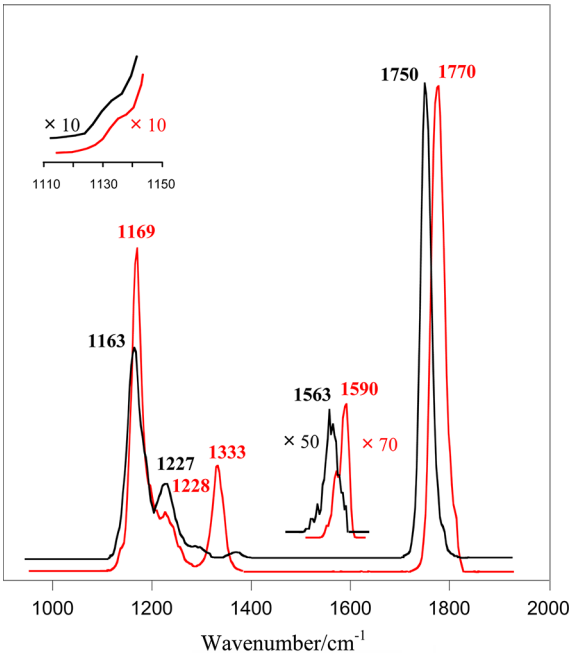

Figure 1. Experimental IRMPD spectra of $HypH^+$ (black trace) and $hypH^+$ (red trace) recorded in the mid-IR region.

The two profiles exhibit nearly exact matching in the low frequency region, with bands (common to the two species) at 1163/1169 and 1227 cm^{-1}. Some notable differences emerge in the high-frequency side, though, with absorptions at 1563 and 1750 cm^{-1} for $HypH^+$ and at 1590 and 1770 cm^{-1} for $hypH^+$. Moreover, a distinct and highly diagnostic band is observed at 1333 cm^{-1} only in the IRMPD spectrum of $hypH^+$. Both spectra present a shoulder at approximately 1132 cm^{-1} on the red side of a peak at 1163/1169 cm^{-1} and an additional one at 1794 ($HypH^+$) and 1803 cm^{-1} ($hypH^+$) on the blue side of the bands at 1750 and 1770 cm^{-1}, respectively.

Vibrational features also have been recorded in the NH/OH stretching region (3200−3700 cm^{-1}) as shown in Figure 2. In this spectral region, the two sampled species share very similar absorptions, with a sharp (fwhm = 12 cm^{-1}), prominent mode at 3551 ($hypH^+$) and 3556 ($HypH^+$) cm^{-1}, a common landmark in the IRMPD spectra of other positively charged amino acids,[73] along with weaker bands at 3320, 3648, 3658, and 3663 cm^{-1} for $HypH^+$ and at 3336, 3646, 3655, and 3663 cm^{-1} for $hypH^+$.

3.3. Computed Structures. To obtain insights into the features of $HypH^+$ and $hypH^+$ and assign their vibrational transitions, theoretical calculations were performed, which allowed us to identify the most stable structures of each sampled ion. All structures present a nonzwitterionic form, with the additional protons placed on the nitrogen atom, which is the most basic site also in native proline.[36,41,74,75] The relevant thermodynamic data including relative enthalpy and free energy values at 298 K (kJ mol^{-1}) are summarized in Table 1.

Figures 3 and 4 illustrate the lowest energy conformers for bare $HypH^+$ and $hypH^+$, respectively, all comprised within a

dx.doi.org/10.1021/jp302382p | J. Phys. Chem. B 2012, 116, 8771−8779

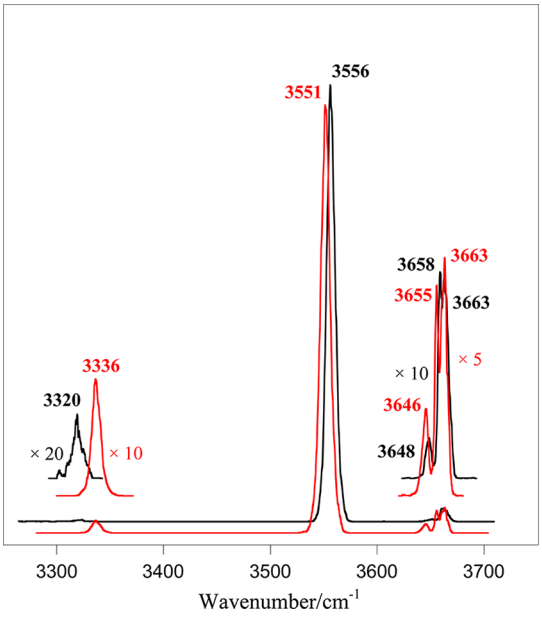

Figure 2. Experimental IRMPD spectra of $HypH^+$ recorded in the higher frequency OH stretch region.

21.4 kJ mol^{-1} energy window (Gibbs free energies at 298 K). A common feature is the *cis*-configuration of the carboxylic group. The two most stable conformers present an ion protonated at the secondary amine group with both H-atoms engaged in hydrogen bonding. The first one binds to the carbonyl oxygen, establishing a C═O···H−N interaction ($r_{O\cdots H}$ = 2.02 Å in $HypH^+$; $r_{O\cdots H}$ = 1.94 Å in $hypH^+$). The second H-atom interacts with the hydroxy substituent in C(4) position, which may be depicted as C(4)−O···H−N ($r_{O\cdots H}$ = 2.68 Å in $HypH^+$; $r_{O\cdots H}$ = 2.68 Å in $hypH^+$). The latter OH substituent can assume different orientations (marked a and b). By combining these features with the 2-fold possibility of bent *endo*- or *exo*-like configuration of the pyrrolidine ring, couples of low-lying rotamers originate with reversed conformational preference, namely, the *exo* ("up") form in protonated 4(*R*)-hydroxyproline (**R-$_{exo}$ Ia**, global minimum, and **R-$_{exo}$ Ib**, lying 0.89 kJ mol^{-1} higher in energy) and the *endo* ("down") form in protonated 4(*S*)-hydroxyproline (**S-$_{endo}$ Ia**, global minimum, and **S-$_{endo}$ Ib**, pratically isoenergetic with regard to their Gibbs free energies). Although occurring in both, the intramolecular C═O···H−N hydrogen bond is clearly shorter, and therefore stronger, in **S-$_{endo}$ Ia** than in **R-$_{exo}$ Ia**. Furthermore, one needs to consider two couples of conformers differing for the orientation of the carboxyl group, rotated so to favor hydrogen bonding between the protonated secondary amine group and the carboxylic hydroxyl group (HO···HN). The ensuing rotamers **R-$_{exo}$ IIa** and **R-$_{exo}$ IIb** are less stable with respect to **R-$_{exo}$ Ia** by 15.3 and 15.4 kJ mol^{-1}, respectively, and likewise **S-$_{endo}$ IIa** and **S-$_{endo}$ IIb** conformers lie 12.3 and 13.8 kJ mol^{-1} higher than **S-$_{endo}$ Ia**, respectively. Notably, all of these conformers are endowed with the C(4)OH group in an axial position as a common feature. Interestingly, in each epimer, a comparable free energy difference separates the global minimum and the corresponding mismatched pucker, that is, 21.4 kJ mol^{-1} in the couple **R-$_{exo}$ Ia**/**R-$_{endo}$ Ia** and 20.8 kJ mol^{-1} in **S-$_{endo}$ Ia**/**S-$_{exo}$ Ia**. The increased energy of both **R-$_{endo}$ Ia** and **S-$_{exo}$ Ia** structures may be related to the equatorial position occupied by C(4)OH, which hampers the formation of one intramolecular hydrogen bond [C(4)O···H−N] and, besides, the *gauche* (synperiplanar) arrangement of the O−C(4)−C(5)−N chain of the pyrrolidine ring. Such stereoelectronic effects from the electronegative 4-hydroxy substituent have been proposed to provide the C(4)-*exo* conformation in 4(*R*)-hydroxyproline and the C(4)-*endo* conformation in 4(*S*)-hydroxyproline with conformational stability and could also contribute to the thermodynamic properties of the protonated species under examination.[76] Alternatively, the bias has been attributed to a larger electronic delocalization in the C(4)-*exo* puckering over its *endo*-counterpart due to an axial-like conformation of the 4(*R*) group.[31]

Table 1. Thermodynamic Data for the Lowest Energy Conformers of Protonated (2*S*,4*R*)-4-Hydroxyproline ($HypH^+$) and (2*S*,4*S*)-4-Hydroxyproline ($hypH^+$) Calculated at the MP2/6-311+G Level of Theory**

species	E^a	$\Delta H_{rel}^{\circ\,b}$	$\Delta G_{rel}^{\circ\,b}$
	$HypH^{+c}$		
R-$_{exo}$ Ia	−475.633574	0	0
R-$_{exo}$ Ib	−475.632731	1.63	0.89
R-$_{exo}$ IIa	−475.627554	15.2	15.3
R-$_{exo}$ IIb	−475.626547	16.1	15.4
R-$_{endo}$ Ia	−475.624777	22.2	21.4
R-$_{endo}$ Ic	−475.620672	33.6	33.6
R-$_{exo}$ IIIa	−475.619573	35.6	34.8
R-$_{exo}$ IIIb	−475.619223	36.2	35.2
R-$_{endo}$ IIa	−475.618561	38.0	37.4
R-$_{endo}$ IIc	−475.613640	51.1	51.1
R-$_{endo}$ IIIa	−475.611248	56.7	55.5
R-$_{endo}$ IIIc	−475.606616	69.4	69.1
	$hypH^{+d}$		
S-$_{endo}$ Ia	−475.632415	0.10	0
S-$_{endo}$ Ib	−475.632522	0	0.06
S-$_{endo}$ IIa	−475.628171	11.6	12.3
S-$_{endo}$ IIb	−475.626763	14.2	13.8
S-$_{exo}$ Ia	−475.623850	22.4	20.8
S-$_{endo}$ Ic	−475.621862	27.9	27.9
S-$_{exo}$ Ic	−475.620016	33.2	32.5
S-$_{endo}$ IIIa	−475.617699	37.5	36.9
S-$_{exo}$ IIa	−475.617408	38.9	37.1
S-$_{endo}$ IIIb	−475.617788	37.6	37.2
S-$_{exo}$ IIc	−475.613211	50.4	49.4
S-$_{exo}$ IIIa	−475.609849	58.0	55.9
S-$_{endo}$ IIIc	−475.608227	62.9	62.7
S-$_{exo}$ IIIc	−475.606262	68.1	67.0

[a]Electronic energy at 0 K in Hartree/particle. [b]Relative enthalpies (ΔH_{rel}°) and Gibbs free energies (ΔG_{rel}°) at 298 K in kJ mol^{-1}. [c]Optimized structures depicted in Figure 3 and Figure 4S in the Supporting Information. [d]Optimized structures depicted in Figure 4 and Figure 5S in the Supporting Information.

Other structures, including mismatched puckering, with a less favorable C(4)−OH orientation (denoted c) and a *trans* geometry of the carboxylic group, are higher in energy (Table 1) and shown in Figures 4S ($HypH^+$) and 5S in the Supporting Information ($hypH^+$). The protonation of the carbonyl group or of the hydroxyl group of either the carboxylic acid or the C(4)-substituent destabilizes the corresponding isomers by more than 100 kJ/mol and therefore will not be further considered.

3.4. Spectral Assignment. A comparison of the IRMPD spectrum of $HypH^+$ along with the calculated IR absorption

dx.doi.org/10.1021/jp302382p | J. Phys. Chem. B 2012, 116, 8771−8779

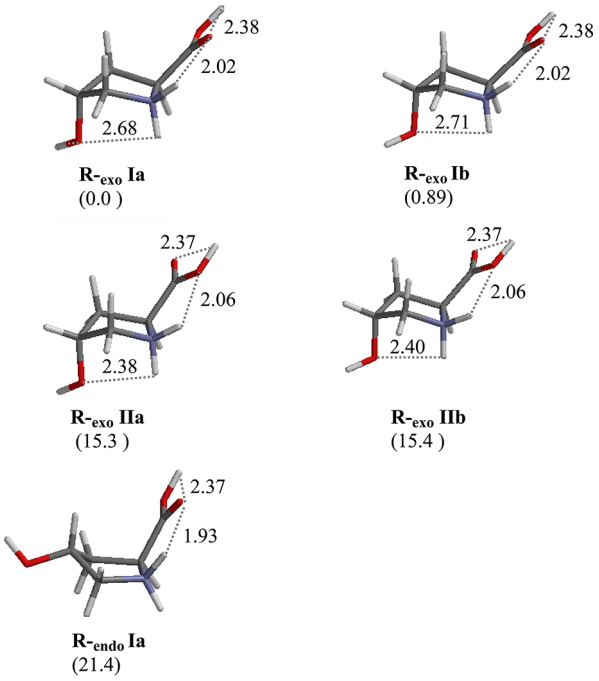

Figure 3. Most stable conformers of protonated (2*S*,4*R*)-4-hydroxyproline ($HypH^+$) and relative free energies (kJ mol^{-1}, in parentheses) at 298 K calculated at the MP2/6-311+G** level of theory. Hydrogen bond lengths, marked by dashed lines, are given in Å.

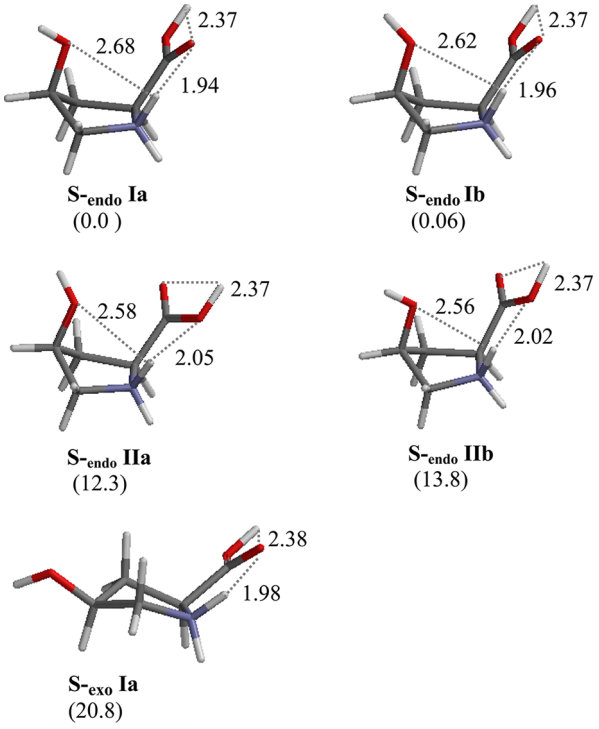

Figure 4. Most stable conformers of protonated (2*S*,4*S*)-4-hydroxyproline ($hypH^+$) and relative free energies (kJ mol^{-1}, in parentheses) at 298 K calculated at the MP2/6-311+G** level of theory. Hydrogen bond lengths, marked by dashed lines, are given in Å.

spectra of the low-lying structures **R-$_{exo}$ Ia**, **R-$_{exo}$ Ib**, **R-$_{exo}$ IIa**, **R-$_{exo}$ IIb**, and **R-$_{endo}$ Ia** are presented in Figure 5, illustrating both the mid-IR and the NH/OH stretching ranges. In a similar

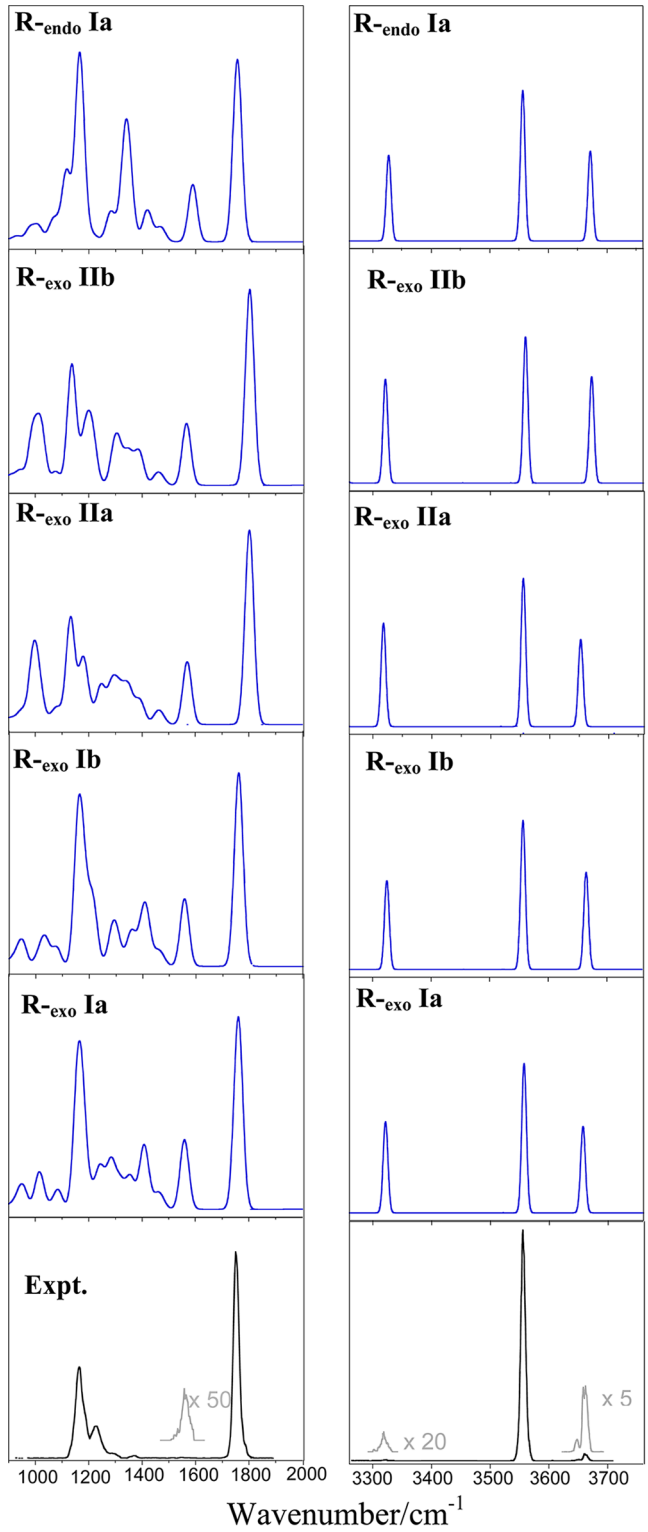

Figure 5. IRMPD spectra of protonated (2*S*,4*R*)-4-hydroxyproline, $HypH^+$ (bottom), and computed IR spectra of conformers **R-$_{exo}$ Ia**, **R-$_{exo}$ Ib**, **R-$_{exo}$ IIa**, **R-$_{exo}$ IIb**, and **R-$_{endo}$ Ia** at the MP2/6-311+G** level of theory.

way, Figure 6 shows the IRMPD spectrum of $hypH^+$ together with the computed IR spectra of candidate isomers **S-$_{endo}$ Ia**, **S-$_{endo}$ Ib**, **S-$_{endo}$ IIa**, **S-$_{endo}$ IIb**, and **S-$_{exo}$ Ia**, covering the two explored regions. The relevant data are listed in Table 2 along with a concise description of the assigned vibrational modes. A

dx.doi.org/10.1021/jp302382p | *J. Phys. Chem. B* 2012, 116, 8771−8779

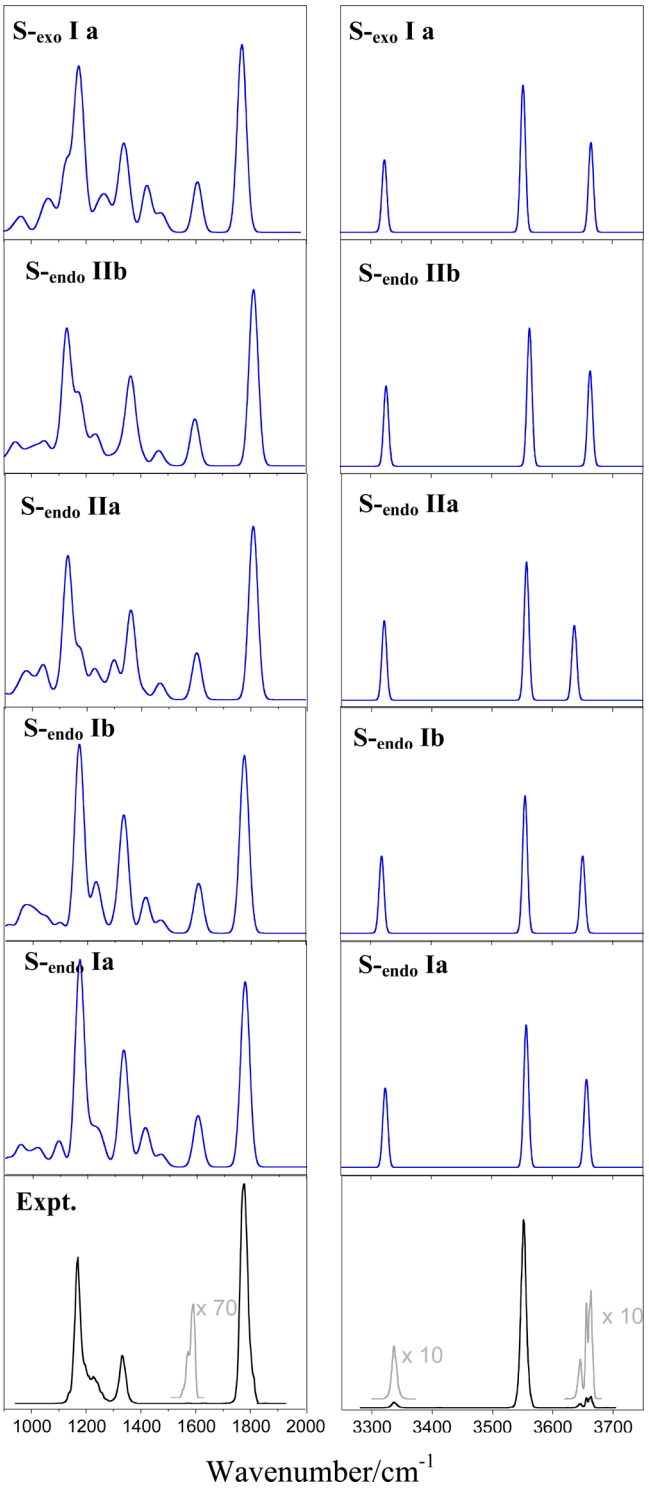

Figure 6. IRMPD spectra of protonated (2*S*,4*S*)-4-hydroxyproline, hypH$^+$ (bottom), and computed IR spectra conformers **S-$_{endo}$ Ia**, **S-$_{endo}$ Ib**, **S-$_{endo}$ IIa**, **S-$_{endo}$ IIb**, and **S-$_{exo}$ Ia** at the MP2/6-311+G** level of theory.

comprehensive presentation of linear IR spectra of all calculated structures is provided in Figures 6S and 7S (HypH$^+$) and Figures 8S and 9S (hypH$^+$) in the Supporting Information.

The good agreement between the experimental and the calculated IR spectra clearly shows that the protonated ions from both epimers may be assigned the lowest energy structures **R-$_{exo}$ Ia** and **S-$_{endo}$ Ia**. Nevertheless, as expected from the close similarity of their structure, which causes a shift of the major IR bands of less than 10 cm^{-1}, other low energy conformers, including **R-$_{exo}$ Ib** and **S-$_{endo}$ Ib**, share very similar absorptions and may well contribute to the sampled ion population.

Among the most active modes for HypH$^+$, the strong band at 1163 cm^{-1} matches with the C−O stretching and COH bending modes due to carboxylic acid group predicted at 1158 cm^{-1}; the weak absorption at 1563 cm^{-1} can be attributed to NH_2 scissoring calculated at 1560 cm^{-1}; the pronounced band at 1750 cm^{-1} corresponds to the C═O stretch expected at 1756 cm^{-1}, and the weak peak recorded at 3320 cm^{-1} matches with the asymmetric NH stretch expected at 3322 cm^{-1}. Similarly, the IRMPD spectrum of hypH$^+$ presents an intense band at 1169 cm^{-1}, consistent with C−O stretching and COH bending modes expected at 1167−1169 cm^{-1}, a weak peak at 1590 cm^{-1} assigned to NH_2 scissoring predicted at 1598 cm^{-1}, a strong band at 1770 cm^{-1} consistent with the carbonyl stretch calculated at 1770 cm^{-1}, and a weak feature at 3336 cm^{-1} due to the NH stretch expected at 3330 cm^{-1}. The remarkable feature of the IRMPD spectrum of hypH$^+$ is an intense band observed at 1333 cm^{-1}, encompassing two IR bands. The first one, associated with CH, NH, and carboxylic OH bending vibrations, is predicted at 1325 cm^{-1}, and the second one, associated to NH_2 wagging and C(4)OH bending, is calculated at 1332 cm^{-1}. These modes are likely to be the signature of the major contributing forms to the hypH$^+$ isomer, **S-$_{endo}$ Ia** and **S-$_{endo}$ Ib**. This intense band is missing in the IRMPD spectrum of HypH$^+$. Consistent with the experimental finding, the most abundant rotamers, notably **R-$_{exo}$ Ia** and **R-$_{exo}$ Ib**, present only two IR absorptions in this region, both of scant activity (less than 30 Km mol^{-1}). One band, associated with a combination of NH_2 wagging and C(4)OH bending, is calculated at 1358 cm^{-1}, and the second feature, associated with NH and carboxylic OH bending, is calculated at 1399 cm^{-1}. Interestingly, for the mismatched, higher lying **R-$_{endo}$ Ia**, which shares a C(4) *endo*-pucker with **S-$_{endo}$ Ia** and **S-$_{endo}$ Ib** and, consequently, a C═O···H−N hydrogen bond shorter than in **R-$_{exo}$ Ia** and **R-$_{exo}$ Ib**, a significant IR activity is again predicted in this region, associated to an intense NH bending vibration calculated at 1342 cm^{-1}.

Furthermore, a distinct feature of HypH$^+$ (relative to hypH$^+$) is attached to the systematic red-shift of highly diagnostic bands, including the NH_2 scissoring (ca. 27 cm^{-1}), C═O stretch (ca. 20 cm^{-1}), and NH stretch (ca. 16 cm^{-1}). This finding may be surprising if one considers that **S-$_{endo}$ Ia** and **S-$_{endo}$ Ib** are endowed with shorter hydrogen bonds than **R-$_{exo}$ Ia** and **R-$_{exo}$ Ib**. However, one should note the characteristics and conformational stiffness of the *endo*-puckered forms. For example, the C═O···H(N) angle for a hydrogen bond in an unconstrained geometry is expected near 120°, whereas it amounts to ca. 90° in the low-lying hypH$^+$ forms. Stereoelectronic effects have been repeatedly reported to play an important role in model peptides containing the proline ring.[19]

Despite the generally fair correspondence between experimental and calculated line positions and intensities of **R-$_{exo}$ Ia** and **R-$_{exo}$ Ib** for HypH$^+$ and of **S-$_{endo}$ Ia** and **S-$_{endo}$ Ib** for hypH$^+$ conformers, the activity of the band at 1563 cm^{-1} (HypH$^+$) and at 1590 cm^{-1} (hypH$^+$) in the respective IRMPD spectra is notably weaker than expected, probably because of a somewhat weaker laser intensity in this range due to the interference of adventitious water vapor.

dx.doi.org/10.1021/jp302382p | *J. Phys. Chem. B* 2012, 116, 8771−8779

Table 2. Observed IRMPD Resonances and Calculated Vibrational Frequencies for Protonated (2*S*,4*R*)-4-Hydroxyproline ($HypH^+$) and (2*S*,4*S*)-4-Hydroxyproline ($hypH^+$)

IRMPD[a]	calcd				
$HypH^+$	**R-$_{exo}$ Ia**[b]	**R-$_{exo}$ Ib**[b]	**R-$_{exo}$ IIa**[b]	**R-$_{exo}$ IIb**[b]	vibrational mode
1163	1158 (132)	1160 (170)	1133 (136)	1138 (154)	COH bend + C−O stretch
	1174 (47)	1177 (49)	1180 (73)		COH bend + NH_2 twisting
	1179 (73)	1187 (44)		1187 (48)	CH_2 twisting
1227	1240 (51)	1221 (50)	1246 (48)	1207 (50)	skeletal flexing, NH bend
1563	1560 (89)	1559 (86)	1570 (80)	1561 (79)	NH_2 scissor
1750	1756 (246)	1755 (247)	1797 (248)	1798 (250)	C=O stretch
3320[c]	3322 (116)	3323 (113)	3322 (132)	3317 (132)	Asym NH stretch
3556[c]	3553 (190)	3553 (190)	3552 (189)	3556 (187)	C(O)O−H stretch
3648[c]			3652 (111)		C(4)O−H stretch
3658[c]	3659 (110)				C(4)O−H stretch
3663[c]		3665 (124)			C(4)O−H stretch
				3674 (136)	C(4)O−H stretch
IRMPD[a]	calcd				
$hypH^+$	**S-$_{endo}$ Ia**[b]	**S-$_{endo}$ Ib**[b]	**S-$_{endo}$ IIa**[b]	**S-$_{endo}$ IIb**[b]	vibrational mode
1169	1167 (196)	1165 (196)	1127 (189)	1124 (178)	COH bend + C−O stretch
	1169 (43)	1175 (40)		1161 (47)	CH_2 twisting
				1174 (53)	
1228	1210 (36)	1224 (44)			skeletal flexing
	1235 (31)				CH_2 twisting + NH wagging
1333	1325 (89)	1327 (47)			CH bend, NH bend
	1332 (63)	1331 (105)	1356 (92)	1351 (59)	NH_2 wagging
1590	1598 (66)	1602 (66)	1596 (62)	1590 (62)	NH_2 scissor
1770	1770 (238)	1769 (236)	1801 (230)	1803 (234)	C=O stretch
3336[c]	3330 (102)	3327 (102)	3331 (105)	3332 (106)	Asym NH stretch
3551[c]	3559 (183)	3559 (182)	3565 (183)	3567 (182)	C(O)O−H stretch
3646[c]			3646 (99)		C(4)O−H stretch
3655[c]		3656 (102)			C(4)O−H stretch
3663[c]	3662 (113)				C(4)O−H stretch
				3671 (126)	C(4)O−H stretch

[a]In cm^{-1}. [b]Calculated vibrational modes for the lowest energy conformers for $HypH^+$ (**R-$_{exo}$ Ia**, **R-$_{exo}$ Ib**, **R-$_{exo}$ IIa**, and **R-$_{exo}$ IIb**) and $hypH^+$ (**S-$_{endo}$ Ia**, **S-$_{endo}$ Ib**, **S-$_{endo}$ IIa**, and **S-$_{endo}$ IIb**) at the MP2/6-311+G** level of theory. The reported intensities given in parentheses are in km mol^{-1}. Bands with and intensity lower than 30 km mol^{-1} are not included. All of the calculated IR frequencies in the 950−1950 cm^{-1} (3200−3700 cm^{-1}) range were scaled by 0.971 (0.945). [c]Frequency region (3200−3700 cm^{-1}) explored with an OPO/OPA laser system.

In the high energy portion of the spectrum, the sharp and prominent band at 3551 cm^{-1} for $hypH^+$ and 3556 cm^{-1} for $HypH^+$ is due to the carboxylic acid OH stretch calculated at 3559 and 3553 cm^{-1}, respectively. Furthermore, an envelope of three weaker and less resolved features associated with the free C(4)O−H stretch is observed at 3648, 3658, and 3663 cm^{-1} ($HypH^+$) and at 3646, 3655, and 3663 cm^{-1} ($hypH^+$). The number and relative intensity of these transitions, which reveal the oxidative modification of proline, support the presence of multiple structures accounting for the sampled ion population of both epimers $HypH^+$ (Figure 10S in the Supporting Information) and $hypH^+$ (Figure 11S in the Supporting Information).

Although the **R-$_{exo}$ Ia** and **R-$_{exo}$ Ib** (Figure 3) as well as **S-$_{endo}$ Ia** and **S-$_{endo}$ Ib** (Figure 4) species show closely similar structures, differ by a small energy gap, and are characterized by a similar C(4)-O···H−N hydrogen bond length, however a notable difference is attached to their H−C(4)−O−H dihedral angles (Φ), describing the orientation of the hydroxyl group installed in proline upon oxidative modification. In particular, Φ values of 46° and −25° are found in **R-$_{exo}$ Ia** and **R-$_{exo}$ Ib**, respectively, whereas Φ values of 29° and −46° are found in **S-$_{endo}$ Ia** and **S-$_{endo}$ Ib**, respectively. Interestingly, this distinct feature is specifically reflected in the OH stretching mode involving the C(4)O−H group and revealed in the high energy portion of the spectrum (Figure 10S and 11S in the Supporting Information).

Furthermore, when additional calculations have been performed improving convergence (opt = tight), each $HypH^+$ conformer, either **R-$_{exo}$ Ia** or **R-$_{exo}$ Ib**, maintained its distinct structure, without falling to a common minimum. The same result has been observed for each $hypH^+$ species, either **S-$_{endo}$ Ia** or **S-$_{endo}$ Ib**.[77]

From the comparative examination of Figures 5 for $HypH^+$, a contribution of **R-$_{exo}$ IIa** clearly emerges besides **R-$_{exo}$ Ia** and **R-$_{exo}$ Ib**, each conformer being characterized by a distinct IR active mode in this spectral region (Table 2). In a similar way, a significant population of conformers **S-$_{endo}$ Ia**, **S-$_{endo}$ Ib**, and **S-$_{endo}$ IIa** accounts for the sampled $hypH^+$ ion, as may be derived from comparison of Figure 6 and as proposed in Table 2.

In agreement with these considerations, the weak shoulder centered at ca. 1132 cm^{-1} in the IRMPD spectra of both epimers may be assigned to the resonance expected at 1133 and 1127 cm^{-1} (C−O stretch + COH bend) for the relatively minor isomers **R-$_{exo}$ IIa** and **S-$_{endo}$ IIa**, respectively. In a similar reasoning, the poorly resolved shoulders at 1794 and 1803 cm^{-1} are compatible with the C=O stretch calculated at 1797

dx.doi.org/10.1021/jp302382p | J. Phys. Chem. B 2012, 116, 8771−8779

and 1801 cm^{-1} for **R-$_{exo}$ IIa** and **S-$_{endo}$ IIa**, respectively. Taking into account the relative band intensities, the **R-$_{exo}$ Ia** and **R-$_{exo}$ Ib** conformers, associated with the peaks at 3658 and 3663 cm^{-1}, respectively, seem to prevail, while **R-$_{exo}$ IIa**, related to the band at 3648 cm^{-1}, is only a minor constituent. In analogy, the **S-$_{endo}$ Ia** and **S-$_{endo}$ Ib** structures, associated with the bands at 3663 and 3655 cm^{-1}, respectively, are dominant, while **S-$_{endo}$ IIa**, related to the absorption at 3646 cm^{-1}, is present in much smaller amount. Conversely, any significant contribution of structures **R-$_{exo}$ IIb** ($HypH^+$) and **S-$_{endo}$ IIb** ($hypH^+$) can be discarded because no IRMPD intensity due to the highly active C(4)O−H stretching mode expected at either 3674 or 3671 cm^{-1}, respectively, is observed (Table 2).

Likewise, if the mismatched **R-$_{endo}$ Ia** form were present in the sampled ion population for $HypH^+$, clear absorptions at 3673 cm^{-1}, due to C(4)O−H stretch, at 1342 cm^{-1}, attributed to C−H and N−H bending and at 1118 cm^{-1}, assigned to C(4)−OH stretch, should appear in the IRMPD spectra, in contrast with the lack of experimental evidence (Figure 5). In a similar way, a significant contribution of structure **S-$_{exo}$ Ia** to the IRMPD spectrum of $hypH^+$ can be ruled out, because no features are found at 3670 and 1124 cm^{-1}, where C(4)O−H and C(4)−OH stretches, respectively, are predicted to absorb (Figure 6). As a whole, the experimental results suggest that the mismatched isomers **R-$_{endo}$ Ia** and **S-$_{exo}$ Ia** are not present in the sampled ion population in any significant amount and demonstrate that **R-$_{exo}$ Ia**, **R-$_{exo}$ Ib**, and **R-$_{exo}$ IIa** for $HypH^+$ and **S-$_{endo}$ Ia**, **S-$_{endo}$ Ib**, and **S-$_{endo}$ IIa** for $hypH^+$ largely account for the ionic species assayed by IRMPD at the temperature of the experiment.

4. CONCLUSION

Vibrational spectra of protonated diastereomers (2*S*,4*R*)-4-hydroxyproline ($HypH^+$) and (2*S*,4*S*)-4-hydroxyproline ($hypH^+$) have been recorded in both the 950−1950 and the 3200−3700 cm^{-1} regions by IRMPD spectroscopy using either the FEL CLIO or a tabletop IR OPO/OPA laser coupled with ion trap mass spectrometry. The interpretation of the IRMPD spectra has been allowed by comparison with IR linear absorption spectra of the lower-lying equilibrium structures calculated at the MP2/6-311+G** level.

The present results prove that IRMPD spectroscopy at room temperature can provide distinctive features of bare stereoisomers. In the lower frequency region, $HypH^+$ shows some relevant features shifted to the red, namely, the NH_2 scissoring, C═O stretch, and NH stretch, with respect to $hypH^+$, which in turn presents a distinct feature at 1333 cm^{-1} that is absent in the experimental spectrum of the $HypH^+$ stereoisomer.

In the OH stretching range, for both $HypH^+$ and $hypH^+$, the presence of three conformers is detected. All three most stable structures that account for the observed IRMPD spectrum bear the additional proton on the nitrogen atom. The two positively polarized protons on nitrogen interact by hydrogen bonding with either the carbonyl oxygen (C═O···H−N) or the carboxylic hydroxyl group (HO···HN) on one side and with the hydroxy substituent in the C(4) position [C(4)O···H−N] on the other side. According to calculations, while the stable conformers of protonated 4(*R*)-hydroxyproline adopt a C(4)-*exo* puckering, the conformational preference is reversed for protonated 4(*S*)-hydroxyproline, which rather presents a C(4)-*endo* conformation. Such intrinsic puckering tendency, which endows all interested structures with a favorable gauche arrangement of the O−C(4)−C(5)−N bond sequence of the pyrrolidine ring, confirms the same propensity observed in neutral hydroxyproline even when embedded in collagen and its mimics.

■ ASSOCIATED CONTENT

Supporting Information

Figures S1−S9 associated with this article. This material is available free of charge via the Internet at http://pubs.acs.org.

■ AUTHOR INFORMATION

Corresponding Author

*Tel: +39 06 4991 3596. Fax: +39 06 4991 3602. E-mail: mariaelisa.crestoni@uniroma1.it.

Notes

The authors declare no competing financial interest.

■ ACKNOWLEDGMENTS

We are grateful to Philippe Maitre, V. Steinmetz, Jean-Michel Ortega, and the CLIO team. Financial support by the CNRS (PICS program), by the Italian MIUR (Prin Project No. 2009W2W4YF_004), and by the European Commission through the NEST/ADVENTURE program (EPITOPES, Project No. 15637) is gratefully acknowledged.

■ REFERENCES

(1) *Biochemistry of Collagen*; Ramachandran, G. N., Reddi, A. H., Eds.; Plenum Press: New York, 1976.
(2) Fraser, R. D. B.; MacRae, T. P.; Suzuki, E. *J. Mol. Biol.* **1979**, *129*, 463−481.
(3) Chopra, R. K.; Ananthanarayanan, V. S. *Proc. Natl. Acad. Sci. U.S.A.* **1982**, *79*, 7180.
(4) Bella, J.; Eaton, M.; Brodsky, B.; Berman, H. M. *Science* **1994**, *266*, 75−81.
(5) Holmgren, S. K.; Taylor, K. M.; Bretscher, L. E.; Raines, R. T. *Nature* **1998**, *392*, 666−667.
(6) Kramer, R. Z.; Vitagliano, L.; Bella, J.; Berisio, R.; Mazzarella, L.; Brodsky, B.; Zagari, A.; Berman, H. M. *J. Mol. Biol.* **1998**, *280*, 623−638.
(7) Gorres, K. L.; Raines, R. T. *Crit. Rev. Biochem. Mol. Biol.* **2010**, *45*, 106−124.
(8) Persikov, A. V.; Ramshaw, J. A. M.; Kirkpatrick, A.; Brodsky, B. *Biochemistry* **2000**, *39*, 14960−14967.
(9) Friedman, L.; Higgin, J. J.; Moulder, G.; Robert Barstead, R.; Raines, R. T.; Kimble, J. *Proc. Natl. Acad. Sci. U.S.A.* **2000**, *97*, 4736−4741.
(10) Spickett, C. M.; Pitt, A. R. *Amino Acids* **2012**, *42*, 5−21.
(11) Raines, R. T. *Protein Sci.* **2006**, *15*, 1219−1225.
(12) Inouye, K.; Sakakibara, S.; Prockop, D. J. *Biochim. Biophys. Acta* **1976**, *420*, 133−141.
(13) Steen, H.; Mann, M. *Anal. Chem.* **2002**, *74*, 6230−6236.
(14) Hewitson, K. S.; Schofield, C. J.; Ratcliffe, P. J. *Methods Enzymol.* **2007**, *435*, 25−42.
(15) Vitagliano, L.; Berisio, R.; Mazzarella, L.; Zagari, A. *Biopolymers* **2001**, *58*, 459−464.
(16) Berisio, R.; Vitagliano, L.; Sorrentino, G.; Carotenuto, L.; Piccolo, C.; Mazzarella, L. *Acta Crystallogr., Sect. D: Biol. Crystallogr.* **2000**, *56*, 55−61.
(17) Erdmann, R. S.; Helma Wennemers, H. *Angew. Chem., Int. Ed.* **2011**, *50*, 6835−6838.
(18) Shoulders, M. D.; Raines, R. T. *J. Biol. Chem.* **2011**, *286*, 22905−22912.
(19) Improta, R.; Benzi, C.; Barone, V. *J. Am. Chem. Soc.* **2001**, *123*, 12568−12577.
(20) Eberhardt, E. S.; Panasik, N., Jr.; Raines, R. T. *J. Am. Chem. Soc.* **1996**, *118*, 12261−12266.

(21) O'Hagan, D.; Bilton, C.; Howard, J. A.; Knight, L.; Tozer, D. J. *J. Chem. Soc., Perkin Trans.* **2000**, *2*, 605−607.
(22) Shoulders, M. D.; Kotch, F. W.; Choudhary, A.; Guzei, I. A.; Raines, R. T. *J. Am. Chem. Soc.* **2010**, *132*, 10857−10865.
(23) Hodges, J. A.; Raines, R. T. *J. Am. Chem. Soc.* **2003**, *125*, 9262−9263.
(24) Shoulders, M. D.; Hodges, J. A.; Raines, R. T. *J. Am. Chem. Soc.* **2006**, *128*, 8112−8113.
(25) DeTar, D. F.; Luthra, N. P. *J. Am. Chem. Soc.* **1977**, *99*, 1232−1244.
(26) Haasnoot, C. A. G.; De Leeuw, F. A. A. M.; De Leeuw, H. P. M.; Altona, C. *Biopolymers* **1981**, *20*, 1211−1245.
(27) Abil, E.; Aliev, A. E.; Denis Courtier-Murias, D. *J. Phys. Chem. B* **2007**, *111*, 14034−14042.
(28) Kim, W.; Hardcastle, K. I.; Conticello, V. P. *Angew. Chem., Int. Ed.* **2006**, *45*, 8141−8145.
(29) Cadamuro, S. A.; Reichold, R.; Kusebauch, U.; Musiol, H.-J.; Renner, C.; Tavan, P.; Moroder, L. *Angew. Chem., Int. Ed.* **2008**, *47*, 2143−2146.
(30) Erdmann, R. S.; Wennemers, H. *J. Am. Chem. Soc.* **2010**, *132*, 13957−13959.
(31) Improta, R.; Benzi, C.; Barone, V. *J. Am. Chem. Soc.* **2001**, *123*, 12568−12577.
(32) Improta, R.; Mele, F.; Crescenzi, O.; Benzi, C.; Barone, V. *J. Am. Chem. Soc.* **2002**, *124*, 7857−7865.
(33) Benzi, C.; Improta, R.; Scalmani, G.; Barone, V. *J. Comput. Chem.* **2002**, *23*, 341−350.
(34) Tarakeshwar, P.; Manoragan, S. *J. Mol. Struct. (Theochem)* **1996**, *365*, 167−181.
(35) Ramek, M.; Kelterer, A.-M.; Nikolic, S. *Int. J. Quantum Chem.* **1997**, *65*, 1033−1045.
(36) Marino, T.; Russo, N.; Tocci, E.; Toscano, M. *J. Mass Spectrom.* **2001**, *36*, 301−305.
(37) Marino, T.; Russo, N.; Toscano, M. *J. Phys. Chem. B* **2003**, *107*, 2588−2594.
(38) Czinki, E.; Csaszar, A. G. *Chem.—Eur. J.* **2003**, *9*, 1008−1019.
(39) Lesarri, A.; Cocinero, E. J.; López, J. C.; Alonso, J. L. *J. Am. Chem. Soc.* **2005**, *127*, 2572−2579.
(40) Lesarri, A.; Mata, S.; Cocinero, E. J.; Blanco, S.; López, J. C.; Alonso, J. L. *Angew. Chem., Int. Ed.* **2002**, *41*, 4673−4676.
(41) Wu, R. H.; McMahon, T. B. *ChemPhysChem* **2008**, *9*, 2826−2835.
(42) Wu, R.; McMahon, T. *J. Am. Chem. Soc.* **2007**, *129*, 4864−4865.
(43) Kapota, C.; Lemaire, J.; Maitre, P.; Ohanessian, G. *J. Am. Chem. Soc.* **2004**, *126*, 1836−1842.
(44) Drayss, M. K.; Blunk, D.; Oomens, J.; Schäfer, M. *J. Phys. Chem. A* **2008**, *112*, 11972−11974.
(45) Bush, M. F.; Oomens, J.; Saykally, R. J.; Williams, E. R. *J. Am. Chem. Soc.* **2008**, *130*, 6463−6471.
(46) Wu, R. H.; McMahon, T. B. *Angew. Chem., Int. Ed.* **2007**, *46*, 3668−3671.
(47) Sleno, L.; Volmer, D. A. *J. Mass Spectrom.* **2004**, *39*, 1091−1112.
(48) Oomens, J.; Sartakov, B. G.; Meijer, G.; von Helden, G. *Int. J. Mass Spectrom.* **2006**, *254*, 1−19.
(49) MacAleese, L.; Maitre, P. *Mass Spectrom. Rev.* **2007**, *26*, 583−605.
(50) Eyler, J. R. *Mass Spectrom. Rev.* **2009**, *28*, 448−467.
(51) Polfer, N. C.; Oomens, J. *Mass Spectrom. Rev.* **2009**, *28*, 468−494.
(52) Polfer, N. C. *Chem. Soc. Rev.* **2011**, *40*, 2211−2221.
(53) Oh, H.; Breuker, K.; Sze, S. K.; Ge, Y.; Carpenter, B. K.; McLafferty, F. W. *Proc. Natl. Acad. Sci. U.S.A.* **2002**, *99*, 15863−15868.
(54) Bush, M. F.; O'Brien, J. T.; Prell, J. S.; Wu, C.-C.; Saykally, R. J.; Williams, E. R. *J. Am. Chem. Soc.* **2009**, *131*, 13270−13277.
(55) Fridgen, T. D. *Mass Spectrom. Rev.* **2009**, *28*, 586−607.
(56) Prazeres, R.; Glotin, F.; Insa, C.; Jaroszynski, D. A.; Ortega, J. M. *Eur. Phys. J. D* **1998**, *3*, 87−93.
(57) Oepts, D.; van der Meer, A. F. G.; van Amersfoort, P. W. *Infrared Phys. Technol.* **1995**, *36*, 297−308.
(58) Milko, P; Roithova, J.; Schroeder, D.; Lemaire, J.; Schwarz, H.; Holthausen, M. C. *Chem.−Eur. J.* **2008**, *14*, 4318−4327.
(59) Bouchoux, G.; Salpin, J. Y.; Leblanc, D. *Int. J. Mass Spectrom. Ion Processes* **1996**, *153*, 37−48.
(60) Lemaire, J.; Boissel, P.; Heninger, M.; Mauclaire, G.; Bellec, G.; Mestdagh, H.; Simon, A.; Le Caer, S.; Ortega, J. M.; Glotin, F.; Maitre, P. *Phys. Rev. Lett.* **2002**, *89*, 273002.
(61) Scuderi, D.; Lemaire, J; Maitre, P. *Int. J. Mass Spectrom.* **2006**, *249/250*, 14−20.
(62) Sinha, R. K.; Maitre, P.; Piccirillo, S.; Chiavarino, B.; Crestoni, M. E.; Fornarini, S. *Phys. Chem. Chem. Phys.* **2010**, *12*, 9794−9800.
(63) Merrick, J. P.; Moran, D.; Radom, L. *J. Phys. Chem. A* **2007**, *111*, 11683−11700.
(64) Steill, J.; Zhao, J.; Siu, C.-K.; Ke, Y.; Verkerk, U. H.; Oomens, J.; Dunbar, R. C.; Hopkinson, A. C.; Siu, K. W. M. *Angew. Chem., Int. Ed.* **2008**, *47*, 9666−9668.
(65) Dopfer, O.; Solca, N.; Lemaire, J.; Maitre, P.; Crestoni, M. E.; Fornarini, S. *J. Phys. Chem. A* **2005**, *109*, 7881−7887.
(66) Simon, A.; MacAleese, L.; Maitre, P.; Lemaire, J.; McMahon, T. B. *J. Am. Chem. Soc.* **2007**, *129*, 2829−2840.
(67) Fung, Y. M. E.; Besson, T.; Lemaire, J.; Maitre, P.; Zubarev, R. A. *Angew. Chem., Int. Ed.* **2009**, *48*, 8340−8342.
(68) Prell, J. S.; Chang, T. M.; Biles, J. A.; Berden, G.; Oomens, J.; Williams, E. R. *J. Phys. Chem. A* **2011**, *115*, 2745−2751.
(69) Chiavarino, B.; Crestoni, M. E.; Fornarini, S.; Lemaire, J.; Maitre, P.; MacAleese, L. *J. Am. Chem. Soc.* **2006**, *128*, 12553−12561.
(70) Polfer, N. C.; Valle, J. J.; Moore, D. T.; Oomens, J.; Eyler, J. R.; Bendiak, B. *Anal. Chem.* **2006**, *78*, 670−679.
(71) Stefan, S. E.; Ehsan, M.; Pearson, W. L.; Aksenov, A.; Boginski, V.; Bendiak, B.; Eyler, J. R. *Anal. Chem.* **2011**, *83*, 8468−8476.
(72) Dunbar, R. C.; Steill, J. D.; Oomens, J. *J. Am. Chem. Soc.* **2011**, *133*, 1212−1215.
(73) Kamariotis, A.; Boyarkin, O. V.; Mercier, S. R.; Beck, R. D.; Bush, M. F.; Williams, E. R.; Rizzo, T. R. *J. Am. Chem. Soc.* **2006**, *128*, 905−916.
(74) O'Hair, R. J.; Bowie, J. H.; Gronert, S. *Int. J. Mass Spectrom. Ion Processes* **1992**, *117*, 23−36.
(75) Bouchoux, G.; Salpin, J. Y. *Eur. J. Mass Spectrom.* **2003**, *9*, 391−402.
(76) Shoulders, M. D.; Satyshur, K. A.; Forest, K. T.; Raines, R. T. *Proc. Natl. Acad. Sci. U.S.A.* **2010**, *107*, 559−564.
(77) This paragraph reports a few considerations developed after a reviewer's comment.